Acoustic Disturbances in Galaxy Clusters

Ellen G. Zweibel^{1,2}, Vladimir V. Mirnov², Mateusz Ruszkowski³,

Christopher S. Reynolds^{4,5}, H.-Y. Karen Yang^{4,6}, and Andrew C. Fabian⁵

¹ Department of Astronomy, University of Wisconsin-Madison, 475 N Charter St., Madison, WI 53706, USA

² Department of Physics, University of Wisconsin-Madison, 1150 University Ave., Madison, WI 53706, USA

³ Department of Astronomy, University of Michigan, Ann Arbor, MI 48109, USA

⁴ Department of Astronomy, University of Maryland, College Park, MD 20742, USA

⁵ Institute of Astronomy, University of Cambridge, Cambridge CB3 OHA, UK

**Received 2018 February 11; revised 2018 March 21; accepted 2018 March 22; published 2018 April 26

Abstract

Galaxy cluster cores are pervaded by hot gas which radiates at far too high a rate to maintain any semblance of a steady state; this is referred to as the cooling flow problem. Of the many heating mechanisms that have been proposed to balance radiative cooling, one of the most attractive is the dissipation of acoustic waves generated by active galactic nuclei. Fabian et al. showed that if the waves are nearly adiabatic, wave damping due to heat conduction and viscosity must be well below standard Coulomb rates in order to allow the waves to propagate throughout the core. Because of the importance of this result, we have revisited wave dissipation under galaxy cluster conditions in a way that accounts for the self-limiting nature of dissipation by electron thermal conduction, allows the electron and ion temperature perturbations in the waves to evolve separately, and estimates kinetic effects by comparing to a semicollisionless theory. While these effects considerably enlarge the toolkit for analyzing observations of wavelike structures and developing a quantitative theory for wave heating, the drastic reduction of transport coefficients proposed in Fabian et al. remains the most viable path to acoustic wave heating of galaxy cluster cores.

Key words: galaxies: clusters: intracluster medium - plasmas - waves

1. Introduction

Unopposed radiative cooling in the intracluster medium (ICM) leads to catastrophic mass accretion rates of up to a thousand solar masses per year (Fabian & Nulsen 1977). This constitutes the classic cooling flow problem. Accretion rates predicted by this model are much larger than those inferred from X-ray observations of clusters (e.g., Peterson et al. 2003). Moreover, the central temperature does not fall below \sim keV, and the star formation rates are significantly lower than predicted by the cooling flow model (e.g., Hoffer et al. 2012; Donahue et al. 2015).

Several ICM heating mechanisms have been proposed to offset radiative cooling losses in order to solve the cooling flow problem. Below we list various heating mechanisms considered in the literature, discuss their limitations, and identify a few of the most promising ones. New developments in the field suggest that alternative heating modes that incorporate plasma effects that go beyond pure hydrodynamics may be needed to better explain ICM heating. One such mechanism is the dissipation of acoustic waves excited by the supermassive black holes in cluster centers, which is the main focus of this paper.

1.1. ICM Heating Mechanisms

1.1.1. Thermal Conduction

Thermal conduction from the hot outer ICM regions to the centers of cluster cool cores was considered, e.g., by Zakamska & Narayan (2003). This mechanism lacks a feedback loop that could maintain cluster atmospheres in globally stable states—the models either eventually lead to catastrophic cooling or, if

conduction is strong, to the isothermality of the ICM (e.g., Bertschinger & Meiksin 1986), though thermal runaway may occur on rather long timescales (e.g., Kim & Narayan 2003). Because of the self-limiting nature of heat conduction, Yang & Reynolds (2016a) showed that conductive heating is unlikely to be the dominating heating mechanism even for unsuppressed parallel conductivity. Recent results by Roberg-Clark et al. (2016, 2017), Komarov et al. (2017), and Fang et al. (2018) suggest that the conductive flux may not be linearly proportional to the temperature gradient and that conduction could be severely suppressed compared to the Braginskii level. Thus, conduction on its own does not appear to be a viable solution to the cooling flow problem.

1.1.2. Dynamical Friction and Turbulent Diffusion

Dynamical friction acting on galaxies has been considered by El-Zant et al. (2004) and Kim et al. (2005). While this mechanism can be self-regulating because the heating occurs for supersonically moving galaxies, the models are not thermally stable. Moreover, the minimum temperatures, $\sim T_{\rm vir}$, predicted by this model are larger than observed. While this mechanism is unlikely to provide a complete solution to the cooling flow problem, the onset of thermal instability can be significantly delayed.

Ruszkowski & Oh (2011) suggested that turbulent heat diffusion may lead to efficient heating of cool cores by redistributing the energy from outer parts of the cool cores to the center. In their model, turbulence is excited by galaxy motions and is volume filling due to the excitation of large-scale *g*-modes. The efficiency of turbulent diffusion is boosted by thermal conduction that reduces the stabilizing buoyancy forces. While there exists a parameter regime for which catastrophic cooling can be avoided or significantly delayed,

⁶ Einstein Fellow.

this is unlikely to be a general solution to the cooling flow problem, especially if thermal conduction is significantly suppressed.

1.1.3. Cosmic-Ray Heating

The possibility of heating cool cores by cosmic rays was studied using analytical approaches (Loewenstein et al. 1991; Guo & Oh 2008; Pfrommer 2013; Jacob & Pfrommer 2017a, 2017b) and MHD simulations (Ruszkowski et al. 2017). The emerging consensus from these studies is that cosmic rays may provide sufficient heating to offset radiative cooling even when only a small amount of pressure support in the ICM comes from cosmic rays. While detailed comparisons to the data remain to be performed, these models do not demonstrably violate constraints from radio and gamma-ray observations. Interestingly, these findings are consistent with suggestions by Bambic et al. (2017), who studied turbulence driving in magnetohydrodynamical simulations and argued that turbulence driving is inefficient. They suggest that cosmic rays and sound waves may be necessary to model energy thermalization.

1.1.4. AGN Heating

By far the most promising models to explain the cooling flow problem involve heating by active galactic nuclei (AGNs). This mechanism provides a natural self-regulating feedback loop (e.g., Reynolds et al. 2002; Ruszkowski & Begelman 2002; Guo et al. 2008; Gaspari et al. 2012; Li et al. 2015; Yang & Reynolds 2016b). While the amount of energy supplied by the AGN suffices to offset radiative cooling in cool cores, it is unclear how the AGN energy is distributed and thermalized in the ICM and to what extent the heating is offset by the bubbledriven expansion of the overlying gas (Guo & Mathews 2010). Here we distinguish between three forms of coupling: radiative heating, mechanical heating by turbulent, or incoherent, motions, and mechanical heating or energy transport by coherent flows. Heating by cosmic rays could be considered a fourth type of AGN heating if the cosmic rays are produced by the AGN.

Radiative heating—Radiative heating was studied by a number of authors (e.g., Ciotti & Ostriker 2007; Ciotti et al. 2010), who concluded that both AGN mechanical and radiative feedback are needed to prevent catastrophic cooling flows in elliptical galaxies. Recent results by Xie et al. (2017) suggest that radiative heating could be important in low-luminosity AGNs, where the kinetic feedback mode is typically considered. They suggest that Compton temperatures in these objects can be $\sim\!20$ times higher than previously assumed and, consequently, AGN can heat the gas radiatively.

Turbulent dissipation—Zhuravleva et al. (2014) proposed that dissipation of turbulence could offset radiative cooling inside cool cores. Their approach relies on the conversion of gas density fluctuations to the velocity field. Several simplifying assumptions are made, including isotropic turbulence and the absence of gas density fluctuations associated with dark matter substructure. Such fluctuations could mimic turbulent velocity perturbations. Furthermore, dissipation of heat due to mechanisms not involving turbulence could drive motions, and the dissipation of these motions could be interpreted as turbulent dissipation. While the balance of heating and cooling predicted by this model is very approximate, even perfect balance would not necessarily imply that turbulent dissipation

is the dominant heating mechanism, as the cluster can go though phases of overheating (Li et al. 2017).

Resonant scattering can be used to place further constraints on the turbulent velocity magnitude (e.g., Hitomi Collaboration et al. 2016; Ogorzalek et al. 2017). Lines of abundant ions can have optical depths exceeding unity, and such lines will be attenuated. Turbulence broadens the lines and thus lowers their optical depth and reduces this suppression effect. However, this suppression can be mimicked by predominantly nonturbulent radial gas velocities (Zhuravleva et al. 2011), thus reducing the need for substantial turbulence and associated turbulent dissipation. This could occur if the AGN jet activity is accompanied by a wide-angle wind originating from the vicinity of the central black hole.

In addition to the above caveats concerning the turbulent dissipation model, there are theoretical arguments suggesting that AGNs are not likely to drive enough turbulence in the ICM to offset cooling. Reynolds et al. (2015) isolated the role of incompressible modes (g-modes and turbulence) using controlled numerical experiments and demonstrated that the energy transfer from the AGN to the ICM is insufficient to balance cooling. This claim was corroborated by a more realistic treatment of AGN feedback in global hydrodynamical simulations of cool cores by Yang & Reynolds (2016b), who showed that turbulent dissipation contributes to the heating balance at the level of just a percent. The main heating in their model was due to a combination of shocks and mixing. However, mixing of the thermal bubble gas may be partially inhibited by magnetic fields (Ruszkowski et al. 2007), and the bubbles may be predominantly filled with cosmic rays rather than thermal gas (Dunn & Fabian 2004; Guo & Mathews 2011; Guo 2016). The above considerations suggest that alternative heating modes need to be explored to explain the thermalization of the energy injected by the AGN in the ICM.

A variant on turbulent heating is given in Kunz et al. (2011). This paper is based on the idea that large-scale turbulence in the cluster causes the plasma pressure to become anisotropic with respect to the ambient magnetic field ($p_{\perp} \neq p_{\parallel}$; Schekochihin & Cowley 2006). The level of anisotropy is determined by a balance between turbulent driving and collisional relaxation. If it is assumed that the resulting anisotropy is at the critical level for the mirror ($p_{\perp} > p_{\parallel}$) or firehose ($p_{\perp} < p_{\parallel}$) instability, and that relaxation is due to Coulomb collisions, then the resulting heating rate depends only on the ambient magnetic field strength and plasma temperature, and is argued to be thermally stable.

Shock dissipation—Shocks driven by AGNs have been identified through observations (Randall et al. 2011) and in simulations (Yang & Reynolds 2016b). They tend to form and dissipate close to their source, and are thus a strongly centrally concentrated form of AGN heating. However, the shock-heated gas may propagate energy away from the cluster center through time-dependent flows (Guo et al. 2018) that provide a feedback loop.

There is a close relationship between shock waves and sound waves. Sound waves can steepen into weak shock waves, although geometrical divergence and dissipation counter this effect. On the other hand, the reflection of shock waves from inhomogeneities can produce sound waves. Given their close coupling, sound waves and shock waves should be discussed in tandem.

Sound wave dissipation—Sound waves in the ICM were first reported in the Perseus cluster by Fabian et al. (2003), who suggested that viscous dissipation of the waves could balance cooling. Subsequently, Forman et al. (2005) detected waves in the Virgo cluster. Simulations of ICM heating by viscous dissipation of sound waves were first performed by Ruszkowski et al. (2004a, 2004b), who found that the waves can indeed heat the gas efficiently and propagate to large distances despite somewhat overheating the very central cluster regions. However, as mentioned above, such overheating may not be inconsistent with the data (Li et al. 2017). In the simulations of Ruszkowski et al. (2004a, 2004b), dissipation due to thermal conduction was completely suppressed. Using linear/analytic arguments, Fabian et al. (2005, hereafter F05) suggested that suppression of transport, and in particular thermal conduction, is needed to allow the waves to propagate far from the AGN as is observed. This suppression also allows for better spatial redistribution of the wave energy without overheating the ICM.

Additional arguments in favor of sound wave dissipation come from recent Hitomi constraints on the low level of turbulence in the ICM (Hitomi Collaboration et al. 2016; Fabian et al. 2017). These constraints can be most easily satisfied when sound wave dissipation is invoked because the velocity perturbations associated with sound waves are significantly subsonic. However, ZuHone et al. (2017) show that projection effects could hide faster motions. In their analysis, they simultaneously account for the appearance of the spiral features seen in Perseus and match the line velocity shifts. For different lines of sight, velocities can be larger. The observational results may also be biased toward brighter regions and, consequently, do not constrain the velocities in the lower density gas. Nevertheless, acoustic wave dissipation is a promising mechanism because it is consistent with the Hitomi data and may account for spatially well-distributed heating. While it is not universally agreed that sound waves are generated efficiently in AGN outbursts (Tang & Churazov 2017) and much remains to be understood about the frequency and power spectrum of such waves, there is enough observational and theoretical evidence for such waves to warrant close examination.

The purpose of this paper is to improve the toolkit for studies of acoustic waves in galaxy cluster cores by including physical processes that were omitted from previous work. We solve separate equations for electron and ion temperature perturbations, allowing for the possibility that they differ, and we include ion thermal conduction as well as ion viscosity. We consider the transition in electron behavior from nearly adiabatic to nearly isothermal, and show how this reduces the damping rate. Finally, we consider the transition from collisional to collisionless behavior and compare the predictions of kinetic and fluid theory.

In Section 2, we present basic formulae for Coulomb processes in a hydrogen plasma and evaluate them for densities and temperatures derived for the ICM of the galaxy cluster A2199, the properties of which we will continue to use for numerical examples throughout the paper. In Section 3 and its subsections, we give an overview of wave propagation, derive and solve the dispersion relation in various limits, compare the results with a kinetic theory that includes collisions, and evaluate the electron and ion temperature perturbations. In Section 4, we evaluate the attenuation in amplitude of a propagating wave due to dissipation, and in Section 5, we

evaluate the rates of entropy production by the various dissipation mechanisms. In Section 6, we summarize the results and conclusions.

2. The Collisionality of the ICM

We take a "collision" to be a random event that perturbs the trajectory of a particle. In the cases considered here, each collision has a small effect, and the "collision time" is the time it takes for many collisions to give an rms change of order unity.

The propagation and dissipation of waves depend critically on the collisionality of the medium. Thermal conduction, viscosity, and electron—ion heat exchange all dissipate wave energy and are mediated by collisions. In a collisionless plasma, waves are dissipated when particles absorb wave energy through resonances.

Although the role of interactions between particles and microscale waves is under active study (Kunz et al. 2011; Roberg-Clark et al. 2016, 2017), in this paper we derive most numerical estimates from Coulomb collisions⁷ and describe departures from the Coulomb rates with adjustable parameters as in F05.

Formulae for the electron and ion Coulomb collision times τ_e and τ_i (which is related to τ_e by $\tau_i = \tau_e \sqrt{2M/m}$ for ion and electron masses M, m and $T_e = T_i$) are given in Braginskii (1965, hereafter B65). In evaluating these formulae, we assume a hydrogen plasma, set the Coulomb logarithm $\Lambda = 37$, express the temperature in units of $10^7 {\rm K}$, and use n (in cm⁻³) to denote either n_e or n_i , resulting in

$$(\tau_e, \tau_i) = (2.44 \times 10^8, 1.48 \times 10^{10}) \frac{T_7^{3/2}}{n} \text{s.}$$
 (1)

It is also useful to have the thermal velocities

$$(v_e, v_i) \equiv (\sqrt{k_B T/m}, \sqrt{k_B T/M})$$
 (2)

=
$$(1.23 \times 10^9, 2.87 \times 10^7) T_7^{1/2} \text{cm s}^{-1},$$
 (3)

and mean free paths $\lambda_{e,i} \equiv v_{e,i}\tau_{e,i}$, which are almost the same for the two species,

$$(\lambda_e, \lambda_i) = (3.00, 4.25) \times 10^{17} \frac{T_7^2}{n} \text{cm}.$$
 (4)

In order to describe thermal conductivity and viscosity, we introduce diffusivities $D_{e,i} \equiv \lambda_{e,i}^2 / \tau_{e,i}$,

$$D_{e,i} = (3.69 \times 10^{26}, 1.22 \times 10^{25}) \frac{T_7^{5/2}}{n} \text{ cm}^2 \text{ s}^{-1}.$$
 (5)

We use density and temperature profiles for the cluster A2199 in numerical examples. From Johnstone et al. (2002), $(T_7, n) = (5.0r_2^{0.3}, 6.0 \times 10^{-3}r_2^{-0.75})$, where r_2 is the radius in units of 100 kpc; these formulae hold for $0.05 < r_2 < 2.0$. For A2199, Equations (1) and (4) give in Myr, kpc, and $(\text{kpc})^2/\text{Myr}$, respectively,

$$\log \tau_e = -1.84 + 1.2 \log r_2,\tag{6}$$

The Kunz et al. (2011) assume that the collision frequency is the Coulomb frequency, which implies that the turbulent strain adjusts. Wiener et al. (2017) assume that the collision frequency adjusts while the strain is externally imposed. This leads to an alternative expression for the mean free path which exceeds the Coulomb mean free path for typical cluster core parameters, suggesting that anomalous collisions are not required to maintain the pressure anisotropy at a stable value.

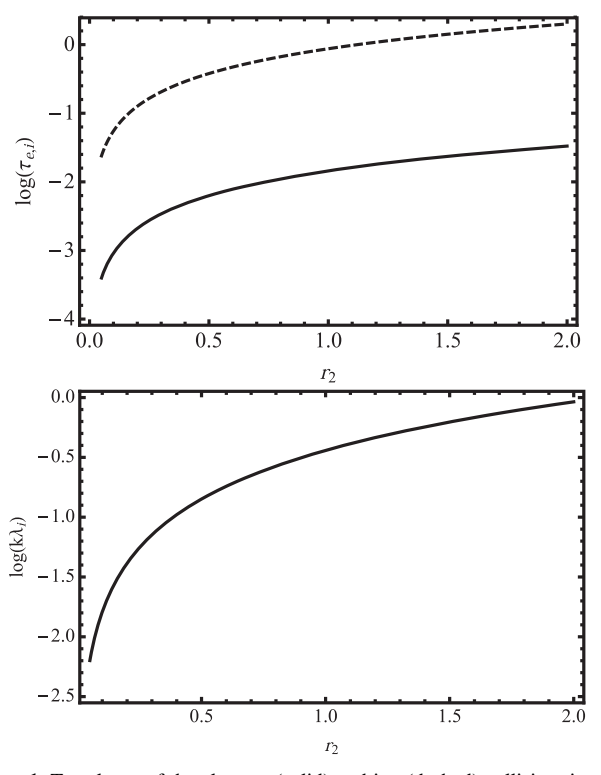


Figure 1. Top: \log_{10} of the electron (solid) and ion (dashed) collision times in Myr as functions of radial position in 100 kpc for the profiles of n and T measured in A2199 by Johnstone et al. (2002). Bottom: \log_{10} of the collisionality parameter $k\lambda_i$ vs. radial position in kpc, assuming a wavelength of 10 kpc, for A2199. The damping rate of such a wave can be estimated accurately with fluid theory within about 100 kpc of the cluster, but should be calculated from kinetic theory beyond this (see Figure 7).

$$\log \tau_i = -0.057 + 1.2 \log r_2,\tag{7}$$

$$\log \lambda_e = -0.392 + 1.35 \log r_2,\tag{8}$$

$$\log \lambda_i = -0.240 + 1.35 \log r_2, \tag{9}$$

$$\log D_e = 1.06 + 1.5 \log r_2,\tag{10}$$

$$\log D_i = -0.420 + 1.5 \log r_2. \tag{11}$$

The electron and ion collision times and the dimensionless parameter $k\lambda_i$ for a wave with wavenumber $k=2\pi/(10\text{kpc})$ for A2199 are plotted in Figure 1.

3. Basic Equations and Dispersion Relation

3.1. Formulation and Estimates

We consider longitudinal $(\mathbf{k} \times \mathbf{u} \equiv 0)$ electrostatic waves of sufficiently low frequency that electron inertia can be ignored. With these assumptions, the wave electron pressure gradient force is almost exactly balanced by the force from the wave electric field. Ion motion is driven by the fluctuating ion pressure gradient and electric field, which due to electron force balance is equivalent to driving by the fluctuating electron pressure gradient. In these low-frequency waves, the electron and ion densities are essentially the same (quasi-neutrality). This is the standard propagation regime for ion acoustic waves in both the fluid and kinetic descriptions, and also holds for the thermal and relaxation waves discussed in Section 3.2. However, although the electrons and ions are tightly coupled dynamically, they are only coupled thermally through collisions, and we will see that in general their temperature perturbations are different.

In a stratified medium with density scale height H, the effect of gravity on sound wave propagation appears through the acoustic cutoff frequency $\omega_{\rm ac} \sim c_s/(2H)$, which sets a lower limit on the frequency of a propagating acoustic wave. For the power-law density profiles considered here, stratification effects are of order $(kr)^{-1} \ll 1$, and we ignore them. Due to the decrease of $\omega_{\rm ac}$ with r, outward propagating waves will not be trapped in an acoustic cavity, but waves generated at large r might be reflected by the acoustic cutoff barrier as they propagate inward.

We also ignore forces due to magnetic fields. This is strictly accurate only for waves propagating parallel to the background magnetic field, but should be a reasonable approximation if the magnetic field is weak, as is thought to be the case in galaxy clusters. However, even a weak field can drastically affect plasma transport processes, and our parameterized modification of the transport coefficients is intended to account for magnetic geometry as well as anomalous collisional processes caused by small-scale electromagnetic fluctuations. Because the cosmicray pressure in galaxy clusters is also thought to be weak, e.g., Aleksić et al. (2012), we also ignore the thermal and dynamical effects of cosmic rays. Finally, we ignore perturbations to the heating and radiative cooling rates because their timescales are long compared to the wave period, because the heating mechanism is unknown, and because it is uncertain whether the cluster gas is in thermal equilibrium at all. We briefly discuss the possible effects of magnetic fields, cosmic rays, and thermal damping/instability in Section 6.

As for our estimates of collisional and thermal parameters, we assume a hydrogen plasma of uniform particle density $n_e = n_i = n$ and temperature $T_e = T_i = T$, and denote the electron and proton masses by m and M, respectively. We introduce $\epsilon \equiv m/M$, which we will treat as a small parameter. With this notation, τ_e/τ_i , v_i/v_e , and D_i/D_e are all of order $\epsilon^{1/2}$.

We expect the wave frequencies and wavenumbers of acoustic waves to be related by $\omega \sim k v_i$, and the characteristic timescales associated with electron thermal conduction, ion thermal conduction, and ion viscosity to be of order $(k^2 D_e)^{-1}$, $(k^2 D_i)^{-1}$, and $(k^2 D_i)^{-1}$. These diffusive processes should be important if their timescales are less than the wave period, or $\omega \tau_i > \epsilon^{1/2}$ for electron thermal conduction and $\omega \tau_i > 1$ for ion thermal conduction or viscosity. But because $\omega \tau_i \sim 1$ is roughly equivalent to $k\lambda_i \sim 1$, kinetic effects, viscosity, and heat conduction for ions all become important at similar wavelengths. In Section 3.3, we show that the ion damping predicted by fluid theory is somewhat larger than that predicted by kinetic theory and is likely an overestimate.

3.2. Fluid Theory

Following the physical picture described in Section 3.1, we represent the plasma by single momentum and continuity equations, but use separate energy equations for the electrons and ions. The evolution of small-amplitude perturbations of a uniform medium is then described by the system of linear equations

$$nM\frac{\partial \boldsymbol{u}_1}{\partial t} = -\boldsymbol{\nabla}(P_{e1} + P_{i1}) - \boldsymbol{\nabla} \cdot \boldsymbol{\pi}_1, \tag{12}$$

$$P_{e1} + P_{i1} = 2n_1T + n(T_{e1} + T_{i1}), (13)$$

$$\frac{\partial n_1}{\partial t} = -n\boldsymbol{\nabla}\cdot\boldsymbol{u}_1,\tag{14}$$

$$\frac{3}{2}\frac{\partial T_{e1}}{\partial t} = -T\boldsymbol{\nabla}\cdot\boldsymbol{u}_1 + \chi_e \nabla^2 T_{e1} - 3\frac{m}{M}\frac{(T_{e1} - T_{i1})}{T_e}, \quad (15)$$

$$\frac{3}{2}\frac{\partial T_{i1}}{\partial t} = -T\boldsymbol{\nabla}\cdot\boldsymbol{u}_1 + \chi_i \nabla^2 T_{i1} + 3\frac{m}{M}\frac{(T_{e1} - T_{i1})}{\tau_e}, \quad (16)$$

where

$$\pi_{1ab} = -\eta_0 \left(\frac{\partial u_{1a}}{\partial x_b} + \frac{\partial u_{1b}}{\partial x_a} - \frac{2}{3} \delta_{ab} \nabla \cdot \boldsymbol{u}_1 \right) \equiv -\eta_0 W_{1ab} \quad (17)$$

is the stress tensor to first order in wave amplitude,

$$\eta_0 \equiv 0.96 nMD_i \tag{18}$$

is the ion viscosity,

$$\chi_e \equiv 3.16D_e \tag{19}$$

is the electron thermal conductivity, and

$$\chi_i \equiv 3.90D_i \tag{20}$$

is the ion thermal conductivity. Ion thermal conduction was not included in F05, but it is of the same order as ion viscosity, so we retain it here. The numerical coefficients multiplying $D_{e,\,i}$ in Equations (17)–(20) are calculated from kinetic theory and taken from B65. We have omitted electron viscosity, which is always a minor effect.

We will want to allow for modified transport coefficients, so we introduce the parameters ξ_{ce} , ξ_{ci} , ξ_{ν} , and ξ_{ei} to multiply χ_e , χ_i , and η_0 , and the electron–ion equilibration term in all of the equations. The parametric approach is undoubtedly an oversimplification: the ξ should be functions that depend on local quantities such as n and T and possibly also on global properties such as magnetic field geometry and level of large-scale turbulence. In fact, the functional forms of the ξ may be critical in closing the feedback loop. However, since we have no theory for the ξ , we adopt simple parameterization here. In principle, the ξ factors could have any magnitude, but we will always assume they suppress transport, i.e., that they lie between 0 and 1.8

We consider solutions of Equations (12)–(16), which depend on t and x as $e^{i(kx-\omega t)}$. We will generally follow F05 in treating ω as known, real, and positive (it represents the frequency at which the waves are driven) and solving for k, which in general is complex: $k = k_r + ik_i$. However, in Section 3.3, we treat k as real and solve for ω to facilitate comparison with results from kinetic theory.

We nondimensionalize the problem by normalizing the first-order quantities such that $(u_1, n_1, T_{e1}, T_{i1}) \rightarrow (u_1/v_i, n_1/n, T_{e1}/T, T_{i1}/T) \equiv (\tilde{u}, \tilde{n}, \tilde{T}_e, \tilde{T}_i)$ and introducing a scaled frequency $\Omega \equiv \omega \tau_i \epsilon^{-1/2}$ and a scaled wavenumber $K \equiv k v_i/\omega$. Ions are collisional $(\omega \tau_i < 1)$ for $\Omega < \epsilon^{-1/2}$, and electrons are collisional for $\Omega < \epsilon^{-1}$. According to the density and temperature profiles we adopted for A2199, waves with 10 Myr periods span the range $0.64 < \Omega < 54$ in $0.05 < r_2 < 2.0$, so we must consider a large range of propagation conditions. Using Equations (13) and (14) in Equations (12), (15), and (16) and assuming plane wave structure we derive the

coupled system

$$[1 - 2K^2 + 1.28i\xi_u \epsilon^{1/2} \Omega K^2] \tilde{n} - K^2 (\tilde{T}_e + \tilde{T}_i) = 0, \quad (21)$$

$$\frac{2}{3}\tilde{n} - [1 + 1.49i\xi_{ce}\Omega K^2]\tilde{T}_e - \frac{2.83i\xi_{ei}}{\Omega}(\tilde{T}_e - \tilde{T}_i) = 0, \quad (22)$$

$$\frac{2}{3}\tilde{n} - [1 + 2.60i\xi_{ci}\epsilon^{1/2}\Omega K^2]\tilde{T}_i - \frac{2.83i\xi_{ei}}{\Omega}(\tilde{T}_i - \tilde{T}_e) = 0,$$
(23)

where we have used the equation of continuity

$$\tilde{n} - K\tilde{u} = 0 \tag{24}$$

to eliminate \tilde{u} .

Equations (21)–(23) describe three distinct linear modes that can be found by standard linear algebra techniques. However, for later purposes (Section 3.2.1) and additional physical insight, we rewrite Equations (22) and (23) in terms of the new variables $\tilde{T} \equiv \tilde{T}_e + \tilde{T}_i$, $\delta \tilde{T} \equiv \tilde{T}_i - \tilde{T}_e$ in terms of which

$$\tilde{T}_i = \frac{1}{2}(\tilde{T} + \delta \tilde{T}),\tag{25}$$

$$\tilde{T}_e = \frac{1}{2}(\tilde{T} - \delta \tilde{T}),\tag{26}$$

Using Equations (25) and (26) in Equations (22) and (23) leads to a pair of equations for \tilde{T} and $\delta \tilde{T}$,

$$\delta \tilde{T} - \frac{i\Omega^2 K^2 c_-}{\Omega + i\Omega^2 K^2 c_+ + 5.66i \xi_{ei}} \tilde{T} = 0, \tag{27}$$

$$(1 + i\Omega K^2 c_+)\tilde{T} - i\Omega K^2 c_- \delta \tilde{T} = \frac{4}{3}\tilde{n}, \qquad (28)$$

where the $c_{\pm} \equiv (1.49\xi_{ce} \pm 2.60\xi_{ci}\epsilon^{1/2})/2$ are proportional to the scaled sum and difference of the electron and ion thermal conductivities. Substituting Equation (27) into (28) and using Equation (24) leads to expressions for both temperature variables in terms of \tilde{n} ,

$$\tilde{T} = \frac{\Omega + i\Omega^2 K^2 c_+ + 5.66i \xi_{ei}}{\mathcal{D}} \frac{4}{3} \tilde{n},\tag{29}$$

$$\delta \tilde{T} = \frac{i\Omega^2 K^2 c_-}{\mathcal{D}} \frac{4}{3} \tilde{n},\tag{30}$$

where

$$\mathcal{D} \equiv \Omega + 2i\Omega^2 K^2 c_+ + \Omega^3 K^4 (c_-^2 - c_+^2) + 5.66i\xi_{ei} (1 + i\Omega K^2 c_+).$$
(31)

Substituting Equation (30) into (21) leads to the dispersion relation

$$[1 - 2K^{2} + 1.28i\xi_{\nu}\epsilon^{1/2}\Omega K^{2}]\mathcal{D}$$

$$= \frac{4}{3}K^{2}(\Omega + i\Omega^{2}K^{2}c_{+} + 5.66i\xi_{ei}). \tag{32}$$

Ignoring all dissipative effects in Equation (32) gives the dispersion relation in the ideal limit

$$1 - \frac{10}{3}K^2 = 0, (33)$$

with solution $K^2 \equiv K_0^2 = 3/10$, as expected for acoustic waves in a $\gamma = 5/3$ gas with mean particle mass M/2.

⁸ The electron–ion thermal coupling parameter ξ_{ei} may be an exception to this; Markevitch & Vikhlinin (2007) argued for anomalously fast T_e , T_i equilibration in cluster shocks. However, it is not clear that the anomalous processes driven in shocks also exist in acoustic waves.

When dissipation is included, Equation (32) is cubic in K^2 and describes three distinct wave modes.

The acoustic mode is of greatest interest here. In the nearly adiabatic limit $\Omega \ll 1$, we can solve for this mode by setting \tilde{T} equal to its adiabatic value perturbed by electron and ion thermal conduction, $(4/3)\tilde{n}/(1+i\Omega K^2c_+)$, in Equation (21) or alternatively keeping only terms proportional to Ω^0 and Ω in Equation (32) and assuming K is order unity. The resulting approximate dispersion relation is

$$1 - \frac{K^2}{K_0^2} = -i\Omega K_0^2 [1.28\xi_{\nu}\epsilon^{1/2} + (1 - 2K_0^2)c_+].$$
 (34)

The imaginary terms in square brackets represent, respectively, ion viscosity and the combined effects of ion and electron thermal conduction. They lead to spatial damping at the rate K_i , which is given to first order in K_i/K_0 by

$$\frac{K_i}{K_0} = \frac{3}{20} \Omega \left[1.28 \xi_{\nu} \epsilon^{1/2} + \frac{2}{5} c_+ \right]
= \Omega(0.0045 \xi_{\nu} + 0.045 \xi_{ce} + 0.0018 \xi_{ci})$$
(35)

or, writing the imaginary part of k in terms of the ion mean free path and substituting numerical values for ϵ and K_0 ,

$$k_i \lambda_i = (\omega \tau_i)^2 (0.105 \xi_{\nu} + 1.03 \xi_{ce} + 0.042 \xi_{ci}).$$
 (36)

Equation (35) agrees with Equation (1) of F05 when written in their notation, except that F05 omitted ion thermal conduction, which increases ion damping by about 40% if $\xi_{\nu} = \xi_{ci}$.

Because Equation (1) of F05 is a weak damping formula, derived assuming the electrons are nearly adiabatic, it overestimates the damping of waves in which conduction is so efficient that the electrons become isothermal. The selflimiting nature of conductive damping is apparent in Figure 2, the top panel of which compares the spatial damping rates derived from the weak damping formula (Equation (35)) with those derived from the full dispersion relation (Equation (32)) for a wave with period 10 Myr propagating in A2199. The bottom panel compares the acoustic mode damping rate when electron-ion collisional coupling is omitted to the value when it is included. Because ion conduction is unimportant for these relatively low values of $\omega \tau_i$ (from Equation (6), $\log \omega \tau_i =$ $1.2 \log r_2 - 0.259 - \log P_7$, where P_7 is the wave period in units of 10 Myr), the ions are nearly adiabatic, and electron collisions with ions prevent the electrons from relaxing to an isothermal state in which there is little dissipation due to electron heat conduction.

The other two modes of the system of Equations (21)–(23) correspond to the relaxation of thermal perturbations. They are nearly isobaric: $2\tilde{n} \sim -\tilde{T}$. Their properties can be derived approximately from Equation (29) by invoking the isobaric condition to replace $4\tilde{n}/3$ by $-2\tilde{T}/3$, which leads to a quadratic equation for K^2 . Here, we give the approximate roots in the limit $\Omega \ll 1$.

One mode, denoted by the superscript (tem), is a temperature wave driven by electron heat conduction. It can be derived without using separate electron and ion energy equations, and has $T_{e1} \sim T_{i1}$. The dispersion relation for the temperature mode is

$$K^{(\text{tem})2} \sim \frac{5i}{3\Omega(0.75\xi_{ce} + 1.30\xi_{ci}\epsilon^{1/2})},$$
 (37)

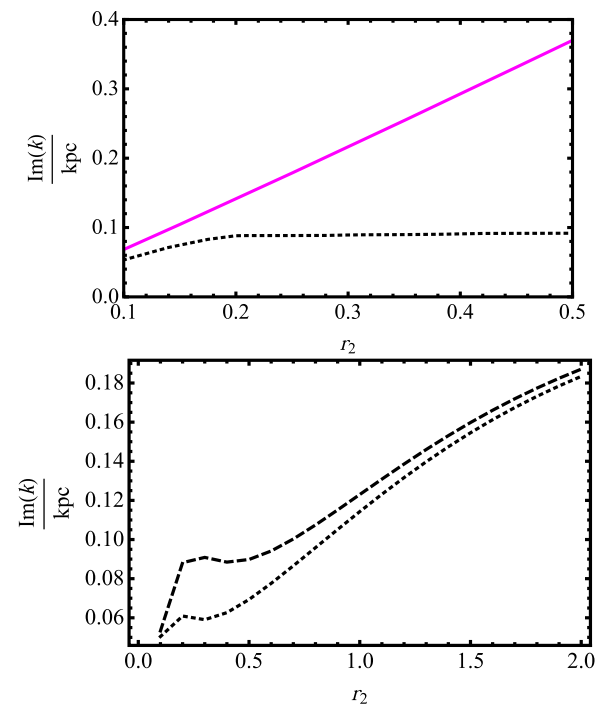


Figure 2. Top: spatial damping rates in units of kpc⁻¹ of acoustic waves with period 10⁷ yr under A2199 conditions computed according to the weak damping formula derived from Equation (35) (magenta curve) and from the full dispersion relation (Equation (32); black dashed curve) when all transport coefficients have their full Coulomb values. The weak damping formula overestimates the damping rate because it assumes nearly adiabatic waves. Bottom: comparison of the spatial damping rates with (long-dashed curve) and without (short dashed curve) electron—ion thermal coupling. When coupling is turned off, electron thermal conduction reduces the electron temperature perturbation, weakening electron thermal conduction damping.

or

$$(k^{\text{(tem)}}\lambda_i)^2 = \frac{0.0389i\omega\tau_i}{(0.75\xi_{ce} + 0.030\xi_{ci})}.$$
 (38)

The temperature mode is excited by entropy perturbations and damps within less than one wavelength of its source. Its characteristic wavelength is the scale on which the heat conduction rate is comparable to the driving frequency.

The other isobaric mode, denoted by the superscript (rel), is driven by electron–ion temperature equilibration. As long as electron heat conduction is much faster than ion heat conduction, electron temperature perturbations quickly relax, so that $T_{e1}/T_{i1}\sim \mathcal{O}(\epsilon)$. The dispersion relation for the relaxation mode is

$$K^{(\text{rel})2} \sim -\frac{1.09\xi_{ei}}{\xi_{..}\epsilon^{1/2}\Omega^2}.$$
 (39)

Or,

$$(k^{\text{(rel)}}\lambda_i)^2 = -0.0254 \frac{\xi_{ei}}{\xi_{...}}.$$
 (40)

The characteristic length scale for this wave is independent of the driving frequency and is set by the length scale at which the ion thermal conduction time equals the electron—ion relaxation time. It is excited by thermal perturbations, which differ between particle species, such as viscous heating of ions in shear flows.

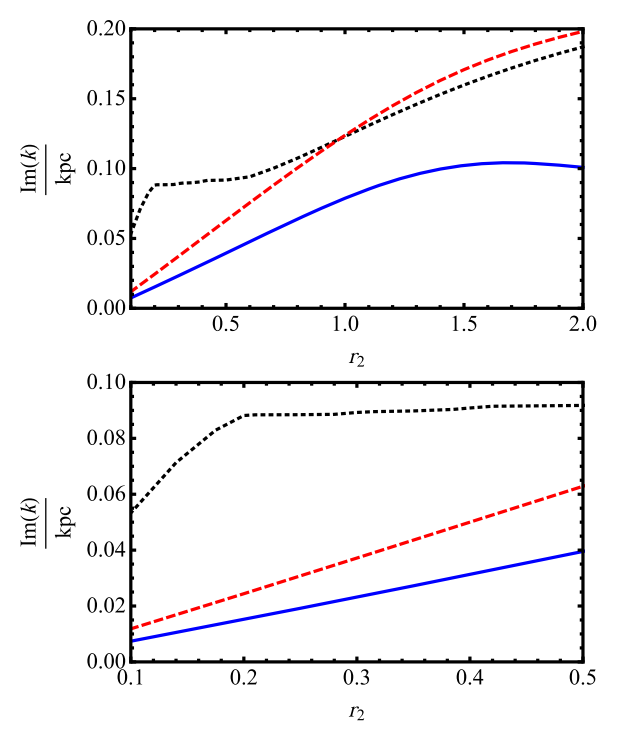


Figure 3. Top: imaginary part of the acoustic wavenumber k in units of kpc⁻¹ for a wave with period 10 Myr as a function of position r_2 in A2199. The curves were computed assuming all transport coefficients have their full Braginskii values (black dotted), electron thermal conduction reduced to 10% of the Braginskii value (red dashed), and both electron thermal conduction and ion viscosity reduced to 10% of their Braginskii values (blue solid). Bottom: same data and styles of curve for the inner 50 kpc of the cluster.

We see from Equations (38) and (40) that both isobaric modes are adequately described by fluid theory ($k\lambda_i \ll 1$) as long as conduction is not too strongly suppressed. It is clear from the large imaginary parts of the isobaric mode wavenumbers that only the acoustic wave can transport energy far from the source. The temperature and relaxation waves damp locally.

Quantitative views of the acoustic wave behavior for A2199 are illustrated in Figure 3. The full transport case (black dotted curve) is the same data that were plotted in Figure 2. The red dashed curve shows the effect of reducing ξ_{ce} to 0.1 while leaving other parameters the same. Although reducing the electron conductivity reduces the damping rate at small r_2 , it delays the onset of electron isothermality, resulting in somewhat elevated damping rates at larger r_2 . Only when both electron conductivity and ion viscosity are reduced to 0.1 their Braginskii values is the damping rate significantly reduced (blue solid curve).

Although many combinations of transport suppression parameters may be possible, there is one particular case that we wish to discuss: a model in which ion viscosity and ion thermal conduction are completely suppressed ($\xi_{\nu} = \xi_{ci} \equiv 0$). This is the limit of very short ion mean free path due to scattering by microinstabilities. It is not obvious that this model is justified in galaxy cluster cores. According to estimates in Wiener et al. (2017) for the core of the Coma cluster, the ion Coulomb mean free path is short enough to suppress the firehose and mirror instabilities that drive microturbulence. However, because this model may be relevant in other environments, because it brings out the effect of electron isothermality, and because, as we show in Section 3.3, the fluid

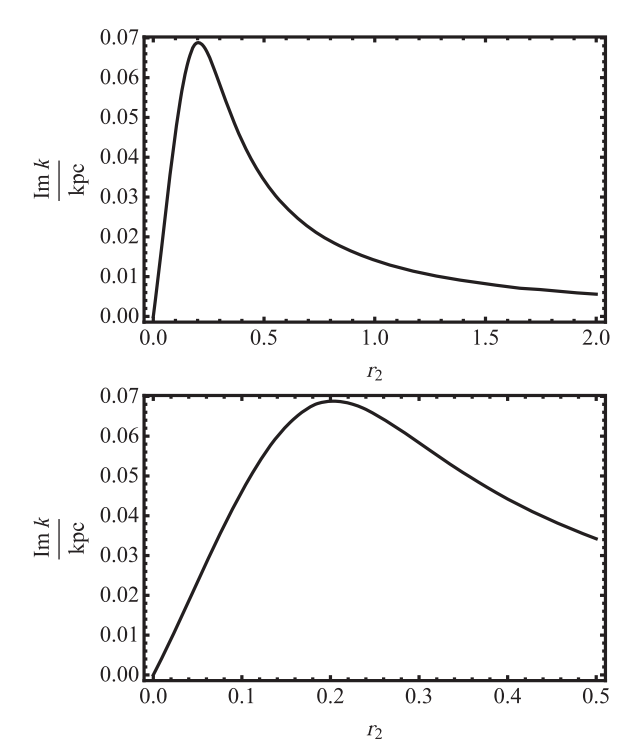


Figure 4. Top: imaginary part of the acoustic wavenumber k in units of kpc⁻¹ for a wave with period 10 Myr as a function of position r_2 in A2199. The curve was computed assuming the electron thermal conductivity and electron—ion temperature equilibration rate have their full Braginskii values, but ion thermal conduction and viscosity are completely suppressed. Bottom: same curve for the inner 50 kpc of the cluster. The peak damping rate occurs at $r_2 \sim 0.22$, where $\Omega \sim 3.85$. This is consistent with the estimate in Section 3.1 for the importance of electron thermal conduction $\omega \tau_i \sim \epsilon^{1/2}$ or $\Omega \sim 1$.

model of ion transport overestimates the damping relative to a more accurate kinetic model, we give results for this model here and build on them throughout the paper.

The reduction in damping as the electrons become isothermal is clearly seen in Figure 4. The peak damping rate occurs at $r_2 \sim 0.22$, where $\Omega \sim 3.85$. This is consistent with the estimate in Section 3.1 for the importance of electron thermal conduction $\omega \tau_i \sim \epsilon^{1/2}$ or $\Omega \sim 1$. In Section 4, we will show that as a result, most of the wave attenuation and heating takes place in the inner part of the domain.

3.2.1. The Temperature Fluctuations

While both ions and electrons contribute to the energy carried by waves, only T_e , which is generally lower than T_i because of the larger electron conductivity, is observable. Fabian et al. (2006) argued for isothermal waves in Perseus, while Zhuravleva et al. (2016) found evidence for adiabatic and isobaric fluctuations as well. Here we discuss the relationships between \tilde{T}_e , \tilde{T}_i , and \tilde{n} in acoustic waves.

The quantity $|\delta T/\tilde{T}|$ is plotted versus Ω in Figure 5 for $0<\Omega<10$. In the adiabatic limit $(\Omega\ll1)$, heat conduction is negligible, and both \tilde{T}_e and \tilde{T}_i are related to \tilde{n} by the usual adiabatic relation $\tilde{T}_e=\tilde{T}_i=2\tilde{n}/3$ for ideal gases. Electron heat conduction becomes more important as Ω increases away from zero, with $|\delta T/\tilde{T}|$ being of order Ω^2 for $\Omega\ll1$. Differences between \tilde{T}_e and \tilde{T}_i become significant for moderate Ω as the electrons become isothermal while the ions remain nearly adiabatic; isothermal electrons but adiabatic ions correspond to $|\delta T/\tilde{T}| \to 1$. At large Ω , the fluid theory should be replaced by

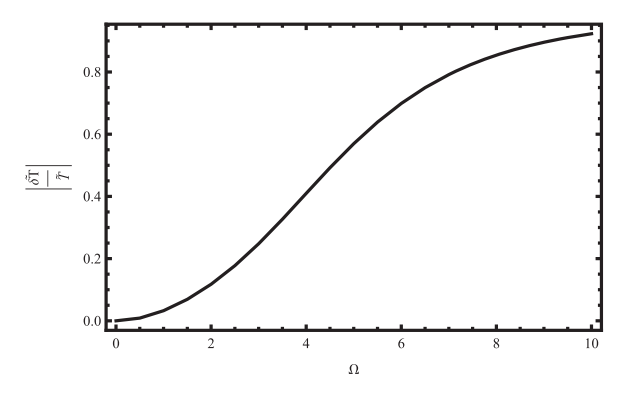


Figure 5. Magnitude of $\delta \tilde{T}/\tilde{T}$, the ratio of the difference to the sum of ion and electron temperature fluctuations defined in Equations (25) and (26), as a function of scaled frequency Ω with all transport coefficients set to their Coulomb values. For $\Omega \ll 1$ ($\omega \tau_i \ll \epsilon^{1/2}$), ions and electrons are well-coupled and the temperature difference is small. As Ω increases above unity, the electrons become more isothermal, and the ratio approaches unity. For even larger Ω , the ions become isothermal as well, and the ratio declines again. As we will see in Section 3.3, the fluid theory is invalid for these large values of Ω .

a semicollisionless or collisionless theory for these large values of Ω (Section 3.3), so we do not extend the plot to large values here.

The magnitude and phase of \tilde{T}_e relative to \tilde{n} are plotted versus Ω in Figure 6. For $\Omega \ll 1$, the waves are almost adiabatic, $\tilde{T}_e/\tilde{n} \sim 2/3$, and the quantities are almost in phase. As Ω increases, the relative amplitude of \tilde{T}_e decreases due to the increasing importance of conduction, and \tilde{T}_e lags \tilde{n} in phase by an increasing amount. The lag is expected for a damped wave; it means that the fluid is losing heat at the time of greatest compression (similar to the damped version of the classic Eddington valve invoked to explain self-excited stellar pulsations). However, the phase shift may be difficult to observe owing to the small amplitude of \tilde{T}_e relative to \tilde{n} in the range of Ω , where the phase shift is large.

3.3. Kinetic Theory

In the collisionless limit $(k\lambda_i \to \infty)$, ion acoustic waves are described by kinetic theory. The electrons are isothermal $(\gamma_e=1)$ and the ions are adiabatic, with one degree of freedom $(\gamma_i=3)$. Collisional damping processes are negligible, and dissipation is primarily due to ion Landau damping: the absorption of wave energy by ions traveling at slightly less than the speed of the wave (electron Landau damping is weaker by a factor of $\epsilon^{1/2}$). Because the wave speed is near the ion thermal speed (unless $T_e\gg T_i$), collisionless damping is strong. The dispersion relation in dimensionless form written for real k and complex ω is

$$\omega \tau_i = (2 - 0.85i)k\lambda_i \tag{41}$$

for $T_e = T_i$. According to Equation (41), ion Landau damping reduces the wave amplitude to 7% of its initial value within one wavelength: ion acoustic waves essentially cannot propagate in a collisionless plasma with $T_e = T_i$.

Ono & Kulsrud (1975) studied the transition from collisional to collisionless behavior by solving the linearized Boltzmann equation with a Fokker–Planck collision operator. They considered only ion–ion collisions and assumed the electrons are isothermal. Therefore, the damping rates they calculated account for ion viscosity and ion thermal conduction, but not for electron thermal conduction or electron–ion temperature relaxation.

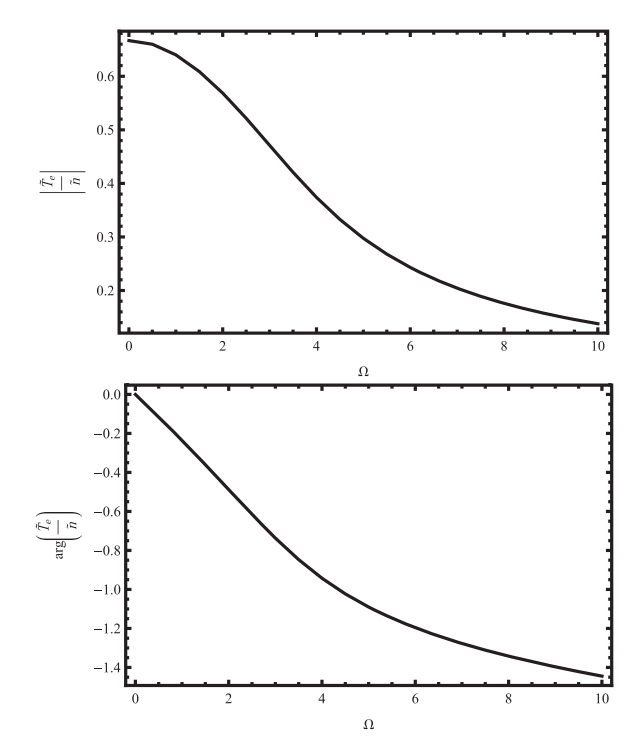


Figure 6. Top: the absolute value of the ratio of the normalized electron temperature perturbation to the normalized density perturbation, $|\tilde{T}_e/\tilde{n}|$ vs. the scaled frequency Ω . For $\Omega \ll 1$, the ratio has the usual adiabatic value of 2/3, but decreases to zero as conduction becomes important at high frequencies, where the electrons are isothermal. Bottom: the phase of \tilde{T}_e/\tilde{n} vs. Ω . As expected for a damped wave, \tilde{T}_e always lags \tilde{n} ; the lag increases with increasing Ω , but the accompanying decrease in $|\tilde{T}_e/\tilde{n}|$ may make the phase lag difficult to detect

In Figure 7, the results of the Fokker–Planck calculation from Table 2 of Ono & Kulsrud (1975; red points connected by a dashed curve to facilitate comparison with fluid models) are compared to the full fluid model (black dashed curve) and a fluid model with isothermal electrons and electron-ion coupling switched off (solid green curve). Note that we have followed Ono & Kulsrud (1975) and computed temporal, not spatial, damping rates. The convergence of the two fluid curves shows that the isothermal electron-adiabatic ion model captures the fluid behavior for $k\lambda_i \lesssim 0.2$. The large blue points mark the values of $k\lambda_i$ at 5 and 100 kpc from the center of A2199. Within this range, the Fokker-Planck and fluid formulae agree to within 20%. Considering the differences between the physical models, this is reasonably good agreement and shows that collisionless effects are small. Comparison of Figure 1 with Figure 2 of Ono & Kulsrud (1975) suggests that the fluid description is adequate within the inner 100–150 kpc of galaxy clusters where acoustic waves are observed.

While we have focused here on the inner parts of the ICM, density and temperature profiles have been measured at larger radii as well. Although both n_e and T generally decline with r, the entropy parameter $T/n_e^{2/3}$ is found to increase with r in a large sample of clusters (Pratt et al. 2010), and λ_i (which is proportional to T^2/n) appears to do so as well. For example, the n_e and T profiles derived by Simionescu et al. (2012) for Perseus give $\lambda_i \sim 20$ –25 kpc at $r_2 \sim 10$. This suggests that acoustic waves launched by dynamical disturbances will damp almost immediately in the outer parts of massive galaxy clusters. Lower mass clusters are cooler and more collisional; for example, the profiles derived for Centaurus by Walker et al.

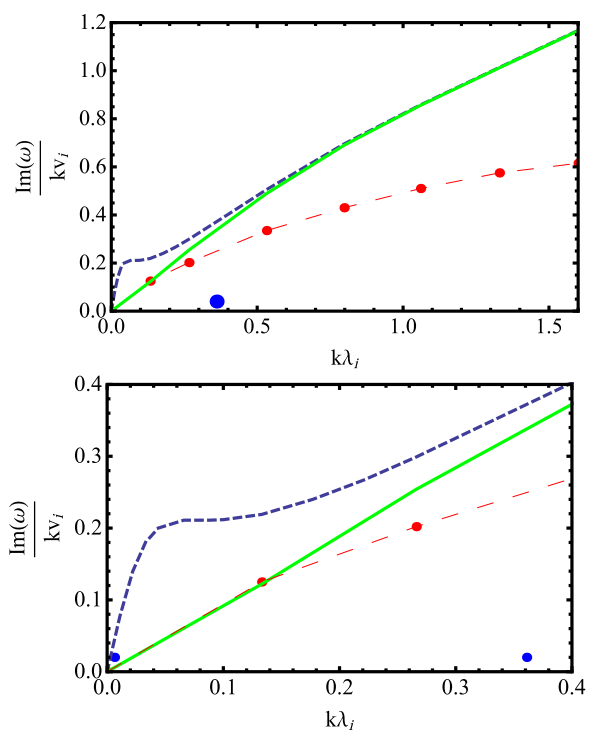


Figure 7. Comparison of the scaled wave damping rate $\text{Im}[\omega]/kv_i$ as a function of $k\lambda_i$ in three different treatments. The top and bottom panels show the same data over different ranges. The black dashed curve is the full fluid dispersion relation. The green curve was obtained from the fluid theory assuming isothermal electrons ($\tilde{T}_e \equiv 0$) and ignoring electron-ion collisional coupling because of its relative slowness. The red points are the damping rates taken from Table 2 of Ono & Kulsrud (1975) and are based on solving the Fokker-Planck equation for ions, accounting for ion-ion collisions only and assuming isothermal electrons. We have added the long-dashed curve to facilitate comparison with the other curves. The blue points show $k\lambda_i$ for A2199 at 5 and 100 kpc from the cluster center. The elevated damping rates at low $k\lambda_i$ seen in the full fluid theory are due to electron thermal conduction. As $k\lambda_i$ and $k\lambda_e$, which is almost the same, increase, the electrons become more isothermal and the damping rates predicted by the green and black dashed curves converge. On the other hand, beyond $k\lambda_i \sim 0.2$, the fluid theory significantly overestimates the damping rate.

(2013) give $\lambda_i \sim 4$ kpc at $r_2 \sim 10$, indicating a more favorable environment for the propagation of waves.

Collisionless acoustic wave damping heats the ions, not the electrons. Using Equation (1) and the relation $\tau_{ei} = \tau_e/\epsilon$, we see that if $T \sim 5$ keV and $n_e \sim 10^{-4}$ cm⁻³, $\tau_{ei} \sim 1.6$ Gyr. This suggests that T_i may exceed T_e in the outer parts of galaxy clusters, making collisionless damping even stronger. It further suggests that pressure models based on T_e may underestimate the ion pressure.

4. Wave Attenuation

Damping attenuates wave amplitude by a factor $\exp(-\mathcal{A}(a, r))$, where

$$\mathcal{A}(a, r) \equiv \int_{a}^{r} k_{i} dr', \tag{42}$$

for a wave launched at a. Equation (42) can be written in terms of the scaled variables as

$$\mathcal{A}(\Omega_a, \, \Omega_r) = \epsilon^{1/2} \int_{\Omega_a}^{\Omega_r} \frac{K_i d\Omega}{v_i d\tau_i / dr},\tag{43}$$

where $\Omega_{a,r}$ are the values of Ω at a and r. If the temperature and density are power laws, $(T, n) \propto (r^{\alpha}, r^{-\beta})$, we can write

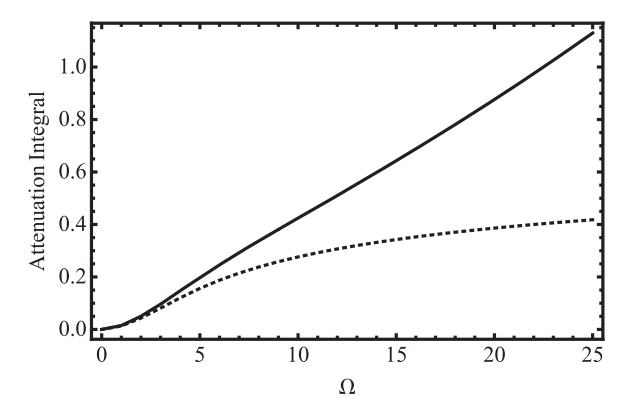


Figure 8. Attenuation integrals $\int_{0.001}^{\Omega} K_i(S) S^{-q} dS$ for q = 0.29, the value derived for A2199, for two transport models. The solid curve represents full Braginskii. The dotted curve shows the effect of completely suppressing ion transport, bringing out the effect of the transition to electron isothermality.

$$(v_i, \tau_i) = (v_{i0} r_2^{\alpha/2}, \tau_{i0} r_2^{(3\alpha+2\beta)/2})$$
. Equation (43) is then
$$\mathcal{A}(\Omega_a, \Omega_r) = \frac{2}{3\alpha + 2\beta} \frac{r}{r_2} \frac{\epsilon^{1/2}}{v_{i0}\tau_{i0}} \left(\frac{\omega \tau_{i0}}{\epsilon^{1/2}}\right)^q \int_{\Omega_a}^{\Omega_r} \frac{K_i d\Omega}{\Omega^q}, \quad (44)$$

where $q \equiv 2(2\alpha + \beta - 1)/(3\alpha + 2\beta)$, and we have used

$$r_2 = \left(\frac{\epsilon^{1/2}\Omega}{\omega \tau_{i0}}\right)^{2/(3\alpha + 2\beta)}.$$
 (45)

For A2199, the profiles of Johnstone et al. (2002) give $\alpha=0.3$, $\beta=0.75$, and q=0.29. The integral in Equation (44) is plotted in Figure 8 for $\Omega(a)=0.001$ (for all practical purposes, the center) out to $\Omega=25$.

With $\tau_{i0} = 2.76 \times 10^{13} \text{ s}$, $v_{i0} = 6.43 \times 10^7 \text{ cm s}^{-1}$, the prefactor multiplying the integral in Equation (44) is $8.52/P_7^{0.29}$, where P_7 is the wave period in units of 10 Myr, and

$$\Omega = \frac{23.7}{P_7} r_2^{1.2}.\tag{46}$$

The attenuation factor A for a wave with $P_7 = 1$ is plotted versus r_2 in Figure 9,

The sensitivity of the attenuation factor to gas temperature depends on the transport model and cluster profiles. If we denote the temperature at the reference level where τ_{i0} is measured by T_0 , then the prefactor in Equation (44) scales as $T_0^{(3q-4)/2}$, or -1.57 for A2199. For a 10% increase in T_0 , this reduces the prefactor to 7.34 for waves with $P_7=1$. On the other hand, Ω scales as $T_0^{3/2}$. For A2199, increasing T_0 by 10% increases $\Omega(0.75)$ for a wave with $T_0=1$ to 19.4, increasing $T_0=1$ from 6.18 to 6.22 in the full Braginskii case and decreasing $T_0=1$ from 3.07 to 2.80 in the full suppression of the ion transport case.

If all forms of transport are so strongly suppressed that the weak damping formula (Equation (35)) applies, the attenuation factor can be written in the form

$$\mathcal{A}(0, r_2) = 607 \left(\frac{10 \text{ Myr}}{P}\right)^2 \xi_{\text{tot}} r_2^{2.05},$$
 (47)

where $\xi_{\text{tot}} \equiv 0.0048 \xi_{\nu} + 0.045 \xi_{ce} + 0.0018 \xi_{ci}$ is a total suppression factor. If all transport coefficients have their full Braginskii values, then $\xi_{\text{tot}} = 0.0516$. Equation (47) can be used to solve for the degree of transport suppression needed to achieve any given attentuation factor. For example, if

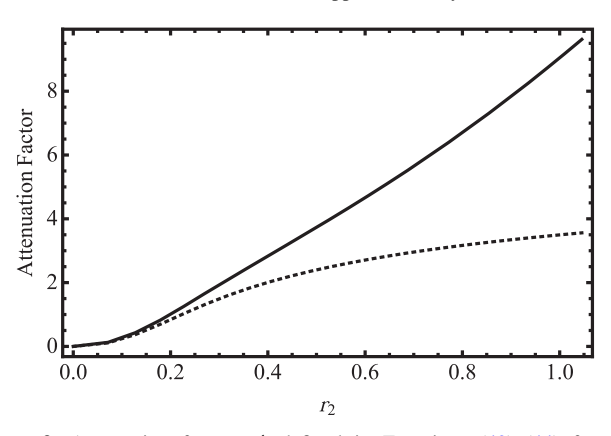


Figure 9. Attenuation factors \mathcal{A} defined in Equations (42)–(44) for two transport models. The solid curve represents full Braginskii. The dotted curve shows the effect of completely suppressing ion transport, bringing out the effect of the transition to electron isothermality (collisional electron—ion temperature coupling is present in the model).

P = 10 Myr, then $\mathcal{A}(0, 0.5) = 1 \text{ if } \xi_{\text{tot}} = 0.0068$, or 13% of the Braginskii value.

5. Heating by Wave Dissipation

The heating rate is given by F05 in terms of an acoustic luminosity $L_s(r)$, which takes the value $L_{\rm inj}$ at an injection radius $r_{\rm inj}$ and is attenuated by dissipation as it travels through the medium according to

$$\frac{dL_s}{dr} = -2k_i L_s. (48)$$

The heating rate per unit volume is

$$\epsilon_{\rm diss} = 2k_i \frac{L_s(r)}{4\pi r^2}.\tag{49}$$

If we define a wave energy flux F_s such that $L_s = 4\pi r^2 F_s$, then Equations (48) and (49) identify the heating rate with the divergence of F_s . Since $k_i \equiv 0$ for an ideal system, the heating rate vanishes without dissipation.

Equation (49) is intuitively plausible, but it has two limitations. One is that it does not separate energy input due to *PdV* work from energy input due to heating. The other is that it can be estimated from, e.g., our understanding of AGN power output (as was done in F05), but not measured directly within the ICM.

To illustrate the first problem, we start with the energy conservation law for the combined electron-ion fluids (B65),

$$\frac{\partial \epsilon}{\partial t} = -\nabla \cdot \boldsymbol{F},\tag{50}$$

where

$$\epsilon \equiv \frac{1}{2}\rho u^2 + \frac{3}{2}(P_e + P_i) \tag{51}$$

is the combined mechanical and thermal electron and ion energy density, and

$$\mathbf{F} \equiv (\epsilon + P_e + P_i)\mathbf{u} + \xi_{\nu}\boldsymbol{\pi} \cdot \mathbf{u} - \xi_{ce}\chi_e \boldsymbol{\nabla} T_e - \xi_{ci}\chi_i \boldsymbol{\nabla} T_i$$
(52)

is a generalized energy flux made up of the mechanical, enthalpy, viscous, and conductive energy fluxes, summed over electrons and ions. Equation (52) can be used to calculate $L_{\rm inj}$, the rate at which an oscillating source transmits energy to the surrounding medium. For simplicity, we consider a spherically symmetric source oscillating around an equilibrium position at r=a. By symmetry, the energy flux is radial: $\mathbf{F} = \hat{r}F$. The energy per solid angle outside the source changes according to

$$\frac{\partial}{\partial t} \int_{a}^{\infty} \epsilon r^{2} dr = \int_{a}^{\infty} \frac{\partial \epsilon}{\partial t} r^{2} dr - \epsilon (a) a^{2} \frac{\partial a}{\partial t}$$
$$= F(a) a^{2} - \epsilon (a) a^{2} u(a), \tag{53}$$

where in the second equality we have used Equation (50), assumed F decays faster than r^{-2} at infinity, as must occur for a damped wave, and identified $\partial a/\partial t$ with u(a). Using Equation (52), we then find for the rate of energy input to the medium

$$\frac{\partial}{\partial t} \int_{a}^{\infty} \epsilon r^{2} dr$$

$$= a^{2} \left[(P_{e} + P_{i})u + \xi_{\nu}(\boldsymbol{\pi} \cdot \boldsymbol{u})_{r} - \xi_{ce} \chi_{e} \frac{\partial T_{e}}{\partial r} - \xi_{ci} \chi_{i} \frac{\partial T_{i}}{\partial r} \right]_{a}.$$
(54)

Equation (54) shows that the global energy is changed by PdV work (the first term on the right-hand side of Equation (54)) and by dissipation (the viscosity and heat conduction terms). The wave contribution to Equation (54) comes from expanding F to second order in the wave amplitude. We will not do that here, except to note that in an ideal medium the pressure and velocity perturbations are out of phase by $\pi/2$, so only a damped or growing wave can do work on its environment (Goldreich & Nicholson 1989).

In order to eliminate the ambiguity between doing work and adding heat, we appeal to the entropy conservation law (B65, Landau & Lifshitz 1987)

$$\frac{\partial S}{\partial t} + \nabla \cdot \left(SV + \frac{q_e + q_i}{T} \right) = \theta, \tag{55}$$

where S is the plasma entropy per volume, \mathbf{q}_e , \mathbf{q}_i are the electron and ion heat fluxes, and $\theta T \equiv T(\theta_\nu + \theta_{ce} + \theta_{ci} + \theta_{ei})$ are the rates of entropy production per volume due to ion viscosity, electron heat conduction, ion heat conduction, and electron—ion collisional heat exchange, respectively. For waves, these heat sources take the forms

$$T\theta_{\nu} = -\frac{1}{2} \xi_{\nu} \pi_{ab} W_{ab} = 1.28 \xi_{\nu} \frac{\rho v_i^2}{\tau_i} (\omega \tau_i)^2 |\tilde{n}|^2, \tag{56}$$

$$T\theta_{ce} = \frac{n\xi_{ce}\chi_{e}}{T}|\nabla T_{e}|^{2} = \frac{2.23}{\epsilon^{1/2}}\xi_{ce}\frac{\rho v_{i}^{2}}{\tau_{i}}|k\lambda_{i}|^{2}|\tilde{T}_{e}|^{2},$$
 (57)

$$T\theta_{ci} = \frac{n\xi_{ci}\chi_i}{T}|\nabla T_{il}|^2 = 3.90\xi_{ci}\frac{\rho v_i^2}{T}|k\lambda_i|^2|\tilde{T}_i|^2,$$
 (58)

$$T\theta_{ei} = 3\xi_{ei} \frac{m}{M} \frac{n}{T\tau_e} (T_{e1} - T_{i1})^2 = 4.24\xi_{ei} \epsilon^{1/2} \frac{\rho v_i^2}{\tau_i} |\tilde{T}_e - \tilde{T}_i|^2,$$
(59)

where the notation comes from Section 2.

The contributions of viscosity, electron and ion heat conduction, and electron—ion thermal coupling to the heating rate computed from Equations (56)–(59) are shown as

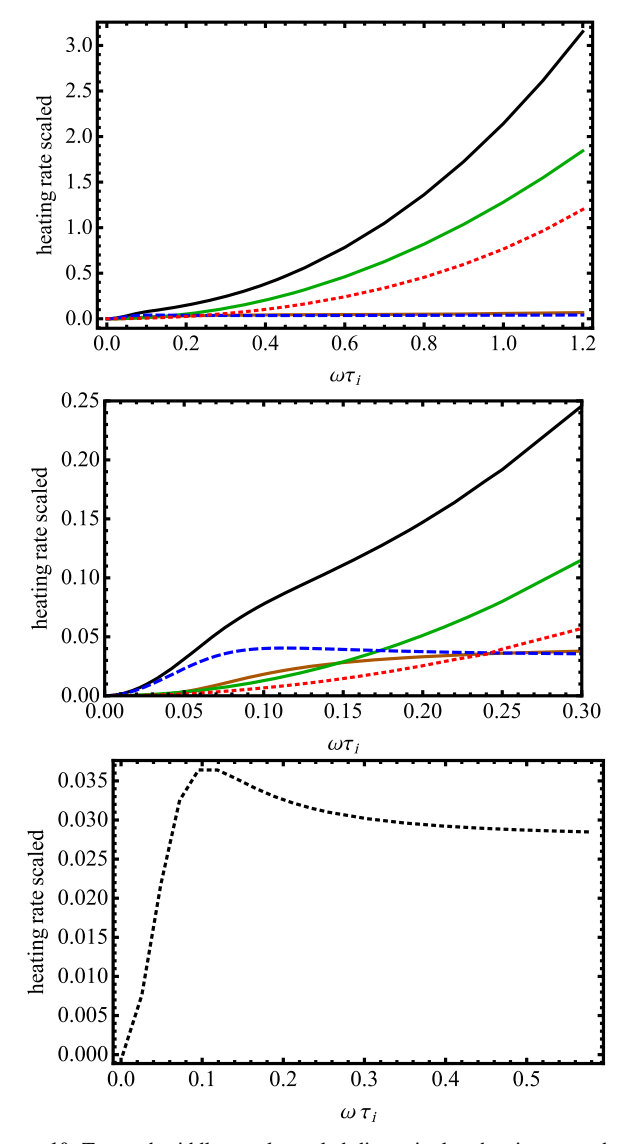


Figure 10. Top and middle panels: scaled dimensionless heating rates due to ion viscosity (solid green curve), ion heat conduction (dotted red curve), electron heat conduction (blue dashed curve), and electron—ion thermal coupling (solid orange curve) from Equations (56) to (59) and their sum, the function Ψ (solid black curve), as functions of the collisionality parameter $\omega \tau_i$ when all transport coefficients have their full values. To convert these rates to energy per volume per time for a wave with density amplitude \tilde{n} , multiply by $\rho v_i^2/\tau_i \tilde{n}^2$. The top and middle panels plot the same data, but the middle panel is zoomed in. The points $\omega \tau_i = 1.2$ and $\omega \tau_i = 0.3$ correspond to $r_2 = 1.92$ and $r_2 = 0.60$, respectively, for a wave with P = 10 Myr. The bottom panel shows the scaled heating rate due to electron thermal conduction when ion transport is completely suppressed. It is very similar to the electron heating rate in the full Braginskii transport case.

functions of $\omega \tau_i$ in the top and middle panels of Figure 10 for the case where all transport coefficients have their full Coulomb values. The total scaled heating rate summed over all contributions is given by the black curve. At small $\omega \tau_i$, electron thermal conduction dominates, but is overtaken by ion heat conduction and viscosity as $\omega \tau_i$ increases beyond a few tenths, mirroring the contributions of these processes to damping. As the electrons approach isothermality, their temperature perturbation \tilde{T}_e is determined by balancing thermal conduction against compression. This leads to $\tilde{T}_e \propto \tilde{n}/k$ and $\nabla \tilde{T}_e$ independent of k, giving a nearly constant rate of entropy production. Ion thermal conduction is relatively unimportant

for the range of $\omega \tau_i$ considered here, so entropy production is nearly quadratic in $\omega \tau_i$ (or k), as is viscous heating. The bottom panel of Figure 10 shows the scaled entropy production rate by electron thermal conduction when ion transport is completely suppressed. It is very similar to the blue dashed curves in the top and middle panels. The location of the peak coincides with the maximum damping rate, which is near $r_2 \sim 0.22$ (see Figure 4).

Although these results are presented in dimensionless form, they are readily converted to physical values. Expressing \tilde{T}_e and \tilde{T}_i in terms of \tilde{n} using Equations (25), (26), (29), and (30), denoting the resulting sum of the coefficients of $(\rho v_i^2/\tau_i)\tilde{n}^2$ in Equations (56)–(59) by Ψ , and using Equation (1), we have

$$\theta T = \Psi \frac{\rho v_i^2}{\tau_i} \tilde{n}^2 = 0.93 \times 10^{-19} n^2 T_7^{-1/2} \Psi \tilde{n}^2 \text{ erg cm}^{-3} \text{ s}^{-1}.$$
(60)

The factor Ψ (which is a function of $\omega \tau_i$) is the black curve plotted in Figure 10.

In following the heating associated with any particular wave propagating outwards from the cluster center, it is important to consider its attenuation. Thus, although entropy production increases outward in the full Braginskii model, this is more than offset by the decreasing amplitude. If ion transport is suppressed, there is very little attenuation and nearly constant entropy production once the wave enters the isothermal regime, resulting in a much flatter heating rate.

Equation (60), because of its n^2 dependence, is readily compared to the optically thin radiative cooling rate to determine, for any temperature, $\omega \tau_i$, and choice of $(\xi_{ce}, \xi_{ci}, \xi_{\nu}, \xi_{ei})$, the wave relative amplitude \tilde{n} such that wave heating balances radiative cooling. Following F05, we write the radiative cooling rate as

$$n^2\Lambda = 10^{-24}n^2(1.13T_7^{-1.7} + 5.3T_7^{0.5} + 6.3) \text{ erg cm}^{-3} \text{ s}^{-1}.$$
 (61)

Combining Equations (60) and (61) gives, for \tilde{n}_{eq} , the wave amplitude at which wave heating balances radiative cooling,

$$\tilde{n}_{\text{eq}} = \frac{3.3 \times 10^{-3}}{\Psi^{0.5}} (1.13T_7^{-1.2} + 5.3T_7 + 6.3T_7^{0.5})^{0.5}. \quad (62)$$

Figure 11 plots \tilde{n}_{eq} as a function of r_2 for a wave period of 10 Myr for the n and T profiles in A2199 and two transport models: full Braginskii (top) and electron thermal conduction only (bottom). While density perturbations as large as 15% can be tolerated without overheating the cluster center, this value drops below 2% at 200 kpc for the full Braginskii case. This is due to the shorter electron and ion collision times at the cluster center, which reduce the transport coefficients and weaken the damping. However, it is an underestimate because the fluid model overestimates viscous damping relative to the kinetic model. Notably, the relative flatness of Ψ in the model without ion transport produces a much flatter curve, as shown in the lower panel of Figure 11.

As shown in Figure 7, kinetic effects reduce the damping rate below the predictions of fluid theory. And, because the heating rates due to ion viscosity and ion thermal conduction scale roughly as ω^2 , increasing the wave period by a factor of 3 would increase \tilde{n}_{eq} by almost the same factor. Nevertheless, our work supports the conclusion reached in F05: in order to

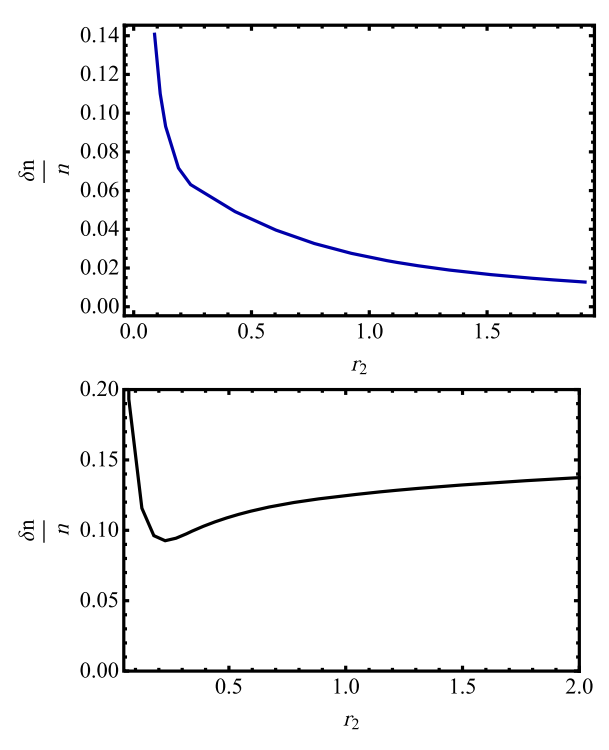


Figure 11. The wave amplitude, measured by the relative density perturbation $\tilde{n} = \delta n/n$, at which radiative cooling balances wave dissipation for a wave with a period of 10 Myr in A2199, computed using the results plotted in Figure 10 according to two transport models: full Braginskii (top) and electron thermal conduction only (bottom). Wave amplitudes above the curve would overheat the cluster; lower amplitudes would underheat it. The top plot underestimates $\delta n/n$ because the viscous damping rates computed from fluid theory are overestimates.

balance wave heating and radiative cooling, transport processes must be strongly suppressed.

Although we have not performed a full stability analysis of acoustic wave heating, Figure 4 and Equation (60) suggest that heating by waves in the full Braginskii model is thermally unstable while heating due to dissipation by electron conduction alone is stable. According to the second equality in Equation (60) the heating rate per volume H for a wave of fixed amplitude $\delta n \equiv n\tilde{n}$ is proportional to $\Psi T^{-1/2}$, while Ψ itself is a function of $\omega \tau_i$, which is proportional to $T^{3/2}/n$. If n and T are perturbed isobarically, such that $\Delta n/n = -\Delta T/T$, then $\Delta\Psi/\Psi = 5/2(\Delta T/T)(\Psi'/\Psi)$, where the prime denotes differentiation with respect to argument. For full Braginskii transport, Ψ increases roughly linearly with $\omega \tau_i$, so $\Delta\Psi/\Psi \sim 5/2(\Delta T/T)$ and $\Delta H/H = 2\Delta T/T$. That is, a positive temperature perturbation increases the heating rate. The same conclusion applies to models with suppressed Braginskii transport. In contrast, Ψ is nearly independent of $\omega \tau_i$ for nearly isothermal acoustic waves, so $\Delta H/H =$ $-1/2(\Delta T/T)$: a positive temperature perturbation decreases the heating rate. This argument should not replace a full stability analysis, however. Although given in terms of local quantities, the analysis here implicitly applies to perturbations on length scales and timescales that are large enough to average over the acoustic waves that are assumed to be supplying the heat. A complete stability analysis of these larger scale perturbations would include the response of the acoustic waves to slow changes in the density and temperature of the medium in which they propagate (Zweibel 1980; Drury & Falle 1986)

as well as perturbations to the radiative cooling rate due to these larger scale perturbations. Global gradients in the background medium should be included as well. These tasks are well beyond the scope of this paper, but could be a promising direction in the future

6. Conclusions

In this paper, we revisited the pioneering study by F05 of acoustic wave dissipation and its effect on thermal balance in galaxy clusters. F05 showed that nearly adiabatic acoustic waves which are damped by plasma thermal conduction and viscosity would damp within one wavelength of their source and overheat the cluster gas if these transport coefficients have the full Braginskii values. Assuming thermal conduction is suppressed entirely and viscosity is reduced to 10% of its Braginskii value allowed a model in which radiative cooling balanced dissipation of a power-law spectrum of waves.

Our results are consistent with those of F05. The wave attenuation due to dissipation can be readily evaluated if transport is so strongly suppressed that the weak damping formula applies (Equation (47)). For example, we found that waves with a 10 Myr period have an *e*-folding length of 50 kpc in A2199 if transport is reduced to 13% of its Braginskii value. Although different combinations of suppression coefficients can achieve this, it requires strong suppression of electron thermal conduction, which accounts for 87% of the total transport in the full Braginskii model.

Here we have focused on enlarging the toolkit for wave heating studies rather than creating a full heating model based on a spectrum of waves. Rather than using a quasi-adiabatic approximation, which applies only for strong collisionality $(\omega \tau_e \ll 1)$, we derived and solved a dispersion relation (Equation (32)) which is based on separate energy equations for electron and ion fluids (Equations (15) and 16), each with its own thermal conductivity and coupled through a Coulomb collision-based energy exchange term. This allows each particle species to transition from adiabatic to isothermal as collisionality decreases (Section 3.2) and yields three modes: the acoustic wave, which is the main topic of this paper, and two nearly isobaric modes, one corresponding to the relaxation of a thermal pulse (Equation (38)), and the other corresponding to electron—ion temperature equilibration (Equation (40)). The isobaric modes are nonpropagating and dissipate their energy within one wavelength of their source.

Conductive damping of acoustic waves is self-limiting: efficient conduction reduces the temperature contrast across the wave and thus reduces the dissipation associated with heat flow. This effect is captured by single fluid theory (e.g., Landau & Lifshitz 1987), but the collisionality at which the transition occurs depends on electron—ion thermal coupling; see Figure 2. For the parameter regimes we studied—wave periods of $\sim\!10$ Myr in the inner 200 kpc of A2199—electrons are isothermal over most of the range if the conductivity has the full Braginskii value while ions are nearly adiabatic. Damping is then due primarily to electron heat conduction near the cluster center, where the gas is most collisional, and to ion thermal conduction and viscosity at lower collisionality and larger radii.

In Section 3.2.1, we evaluated the relative difference between the electron and ion temperature fluctuation and found that for moderate Ω , or $\omega \tau_i > \epsilon^{1/2}$, it can become quite large (Figure 5). Likewise, the electron temperature fluctuation

becomes much smaller relative to the density fluctuation than predicted from adiabatic theory, and δT_e lags δn in phase (Figure 6).

The damping rates, as shown in Figure 2, are lower than the rates computed in the adiabatic approximation of F05, but are still high (Figure 3). At 100 kpc from the center of A2199, for example, waves with a 10 Myr period have been attenuated by more than a factor of e^8 if transport coefficients are at their full Braginskii values (Figure 9). Completely suppressing ion transport reduces the attenuation factor to about 50 if electron thermal conduction is at full strength, which is still large. Partially suppressing electron thermal conduction does result in less attenuation, but the dependence is weak. For example, decreasing the conductivity by a factor of 3 reduces the attenuation factor by only 20%. It is difficult to reconcile these short damping lengths with observations of roughly uniform density enhancements under the propagating acoustic wave interpretation. It is also unlikely that such strongly damped waves could lie within the inertial range of a turbulent

In Section 3.3, we considered kinetic corrections to the fluid picture by comparing the fluid theory to the Fokker–Planck calculation of Ono & Kulsrud (1975; Figure 7). The damping rates calculated according to the fluid and Fokker–Planck models are qualitatively similar, but are higher by \sim 50% in the fluid model under cluster conditions. In the fully collisionless limit ($k\lambda_i \geqslant \sim$ 6), acoustic waves damp within one wave period unless the electron temperature is much higher than the ion temperature. Thus, while kinetic effects somewhat mitigate the rapid damping problem under partial collisionality, they do not solve it completely and imply rapid damping rates in the hottest clusters. In fact, without the strong suppression of collisionless damping, acoustic waves cannot propagate in the outer parts of galaxy clusters.

In Section 5, we evaluated the heating associated with wave dissipation by calculating the rate at which ion viscosity, electron and ion heat conduction, and electron-ion temperature equilibration produce entropy. The relative magnitudes of these entropy sources, shown in Figure (10), track their relative contributions to damping. Electron heat conduction dominates at the highest collisionalities but ion heat conduction and ion viscosity dominate as $\omega \tau_i$ increases, similar to their contributions to damping. Entropy production by electron-ion temperature equilibration is always small. By writing the heating rate in a form explicitly proportional to n^2 (Equation (60)), we were able to solve for the relative density perturbation amplitude $\tilde{n} \equiv \delta n/n$ at which the rate of wave dissipation balances the rate of radiative cooling for a given value of the collisionality parameter $\omega \tau_i$ and ambient temperature T (Equation (62)). The result, plotted in the upper panel of Figure 11 for a 10 Myr period wave in A2199, shows that the equilibrium wave amplitude $\tilde{n}_{\rm eq}$ ranges from about 15% near the cluster center to less than 2% at 200 kpc for the full Braginskii model. However, because the damping rates predicted from the fluid model are higher than the rates predicted from the Fokker-Planck model, the values of \tilde{n}_{eq} computed here are probably underestimates. The model with electron thermal conduction damping only can tolerate a significantly larger wave amplitude without overheating, as seen in the lower panel of Figure 11.

Bearing in mind that our treatment only applies to plane waves in a uniform medium and ignores global geometry,

density, and temperature gradients, we can draw some provisional conclusions. Our calculations reinforce the claim of F05 that without significant suppression of transport, acoustic waves in galaxy cluster plasmas should dissipate within one to two wavelengths of their source. This is in conflict with the interpretation of regularly spaced multiple density ridges as propagating acoustic waves, poses problems for theories of acoustic turbulence with a large inertial range, and puts strict upper limits on wave amplitudes to avoid overheating. How can these problems be resolved?

Magnetic fields, which are undoubtedly present in galaxy clusters, can reduce transport. A large-scale magnetic field perpendicular to the direction of wave propagation almost completely suppresses heat conduction and viscosity, greatly reducing both damping and heating. While this favorable orientation might hold near AGN-driven bubbles due to the sweeping up of the magnetized ICM, it is unlikely to be a solution everywhere in the cluster core. A more general way to reduce transport is to increase the effective collisionality of the medium due to magnetic field fluctuations on small scales. This could occur for electrons due to heat conduction instabilities (Roberg-Clark et al. 2016) and for ions due to pressure anisotropy instabilities (Kunz et al. 2011). As shown in Figures 4, 8, 9, and 10, completely suppressing ion transport results in a dissipation rate that is strongly peaked around the location where the electrons transition from adiabatic to isothermal, reduced attenuation factors, and a relatively flat rate of scaled entropy production with collisionality and, implicitly, with position in the cluster. The numerical examples presented are for waves with a 10 Myr period; the transition occurs closer to or farther from the source depending on whether the wave period is shorter or longer.

It is also possible that the density fluctuations around AGN cavities are driven by a large-scale instability that maintains them despite strong dissipation mechanisms. Cosmic-ray streaming can destabilize acoustic waves (Drury & Falle 1986; Begelman & Zweibel 1994) but requires magnetic field strengths and cosmic-ray pressures that exceed current estimates for galaxy clusters. Further exploration of these and other instabilities, as well as detailed modeling of acoustic wave propagation and damping for realistic galaxy cluster sources and geometries, are topics for future work.

E.G.Z. is happy to acknowledge support from the NSF through grants PHY 0821899 and AST 1616037 and from the University of Wisconsin through the Vilas Trust and WARF Foundation, as well as the hospitality of the University of Chicago, where part of this work was completed. M.R. acknowledges NASA ATP 12-ATP12-0017 grant and NSF grant AST 1715140. C.S.R. thanks NASA for support under grant NNX17AG27G. H.Y.K.Y. acknowledges support from NSF grant AST 1713722, NASA ATP (grant number NNX17AK70G), and the Einstein Postdoctoral Fellowship from NASA (grant number PF4-150129). A.C.F. acknowledges ERC Advanced Grant 340442. We thank the anonymous referee for raising interesting questions and pointing out many salient references.

ORCID iDs

Ellen G. Zweibel https://orcid.org/0000-0003-4821-713X Andrew C. Fabian https://orcid.org/0000-0002-9378-4072

References

```
Aleksić, J., Alvarez, E. A., Antonelli, L. A., et al. 2012, A&A, 541, A99
Bambic, C. J., Morsony, B. J., & Reynolds, C. S. 2017, in AAS/High Energy
   Astrophysics Division Meeting 16, 105.13
Begelman, M. C., & Zweibel, E. G. 1994, ApJ, 431, 689
Bertschinger, E., & Meiksin, A. 1986, ApJL, 306, L1
Braginskii, S. I. 1965, RvPP, 1, 205
Ciotti, L., & Ostriker, J. P. 2007, ApJ, 665, 1038
Ciotti, L., Ostriker, J. P., & Proga, D. 2010, ApJ, 717, 708
Donahue, M., Connor, T., Fogarty, K., et al. 2015, ApJ, 805, 177
Drury, L. O'C., & Falle, S. A. E. G. 1986, MNRAS, 223, 353
Dunn, R. J. H., & Fabian, A. C. 2004, MNRAS, 355, 862
El-Zant, A. A., Kim, W.-T., & Kamionkowski, M. 2004, MNRAS, 354, 169
Fabian, A. C., & Nulsen, P. E. J. 1977, MNRAS, 180, 479
Fabian, A. C., Reynolds, C. S., Taylor, G. B., & Dunn, R. J. H. 2005, MNRAS,
   363, 891
Fabian, A. C., Sanders, J. S., Allen, S. W., et al. 2003, MNRAS, 344, L43
Fabian, A. C., Sanders, J. S., Taylor, G. B., et al. 2006, MNRAS, 366, 417
Fabian, A. C., Walker, S. A., Russell, H. R., et al. 2017, MNRAS, 464, L1
Fang, X-E., Guo, F., Yuan, Y-F., & Mou, G. 2018, arXiv:1801.02160
Forman, W., Nulsen, P., Heinz, S., et al. 2005, ApJ, 635, 894
Gaspari, M., Ruszkowski, M., & Sharma, P. 2012, ApJ, 746, 94
Goldreich, P., & Nicholson, P. 1989, ApJ, 746, 94
Guo, F. 2016, ApJ, 826, 17
Guo, F., Duan, X., & Yuan, Y-F. 2018, MNRAS, 473, 1332
Guo, F., & Mathews, W. G. 2010, ApJ, 712, 1311
Guo, F., & Mathews, W. G. 2011, ApJ, 728, 121
Guo, F., & Oh, S. P. 2008, MNRAS, 384, 251
Guo, F., Oh, S. P., & Ruszkowski, M. 2008, ApJ, 688, 859
Hitomi Collaboration, Aharonian, F., Akamatsu, H., et al. 2016, Natur, 535, 117
Hoffer, A. S., Donahue, M., Hicks, A., & Barthelemy, R. S. 2012, ApJS,
   199, 23
Jacob, S., & Pfrommer, C. 2017a, MNRAS, 467, 1449
Jacob, S., & Pfrommer, C. 2017b, MNRAS, 467, 1478
Johnstone, R. M., Allen, S. W., Fabian, A. C., & Sanders, J. S. 2002, MNRAS,
   336, 299
Kim, W.-T., El-Zant, A. A., & Kamionkowski, M. 2005, ApJ, 632, 157
Kim, W.-T., & Narayan, R. 2003, ApJ, 596, 889
Komarov, S., Schekochihin, A., Churazov, E., & Spitkovsky, A. 2017,
```

arXiv:1711.11462

```
Kunz, M. W., Schekochihin, A. A., Cowley, S. C., Binney, J. J., &
   Sanders, J. S. 2011, MNRAS, 410, 2446
Landau, L. D., & Lifshitz, E. M. 1987, Fluid Mechanics (Amsterdam: Elsevier)
Li, Y., Bryan, G. L., Ruszkowski, M., et al. 2015, ApJ, 811, 73
Li, Y., Ruszkowski, M., & Bryan, G. L. 2017, ApJ, 847, 106
Loewenstein, M., Zweibel, E. G., & Begelman, M. 1991, ApJ, 337, 392
Markevitch, M., & Vikhlinin, A. 2007, PhR, 443, 1
Ogorzalek, A., Zhuravleva, I., Allen, S. W., et al. 2017, MNRAS, 472, 1659
Ono, M., & Kulsrud, R. M. 1975, PhFl, 18, 1287
Peterson, J. R., Kahn, S. M., Paerels, F. B. S., et al. 2003, ApJ, 590, 207
Pfrommer, C. 2013, ApJ, 779, 10
Pratt, G. W., Arnaud, M., Piffaretti, R., et al. 2010, A&A, 511, 85
Randall, S. W., Forman, W. R., Giacintucci, S., et al. 2011, ApJ, 726, 86
Reynolds, C. S., Balbus, S. A., & Schekochihin, A. A. 2015, ApJ, 815, 41
Reynolds, C. S., Heinz, S., & Begelman, M. C. 2002, MNRAS, 332, 271
Roberg-Clark, G. T., Drake, J. F., Reynolds, C. S., & Swisdak, M. 2016, ApJL,
Roberg-Clark, G. T., Drake, J. F., Reynolds, C. S., & Swisdak, M. 2017,
  arXiv:1709.00057
Ruszkowski, M., & Begelman, M. C. 2002, ApJ, 581, 223
Ruszkowski, M., Brüggen, M., & Begelman, M. C. 2004a, ApJ, 611, 158
Ruszkowski, M., Brüggen, M., & Begelman, M. C. 2004b, ApJ, 615, 675
Ruszkowski, M., Enßlin, T. A., Brüggen, M., Heinz, S., & Pfrommer, C. 2007,
   MNRAS, 378, 662
Ruszkowski, M., & Oh, S. P. 2011, MNRAS, 414, 1493
Ruszkowski, M., Yang, H.-Y. K., & Reynolds, C. S. 2017, ApJ, 844, 13
Schekochihin, A. A., & Cowley, S. C. 2006, PhPl, 13, 056501
Simionescu, A., Werner, N., Urban, O., et al. 2012, ApJ, 757, 182
Tang, X., & Churazov, E. 2017, MNRAS, 468, 3516
Walker, S. A., Fabian, A. C., Sanders, J. S., et al. 2013, MNRAS, 432, 554
Wiener, J., Zweibel, E. G., & Oh, S. P. 2017, arXiv:1706.08525
Xie, F.-G., Yuan, F., & Ho, L. C. 2017, ApJ, 844, 42
Yang, H.-Y. K., & Reynolds, C. S. 2016a, ApJ, 818, 181
Yang, H.-Y. K., & Reynolds, C. S. 2016b, ApJ, 829, 90
Zakamska, N. L., & Narayan, R. 2003, ApJ, 582, 162
Zhuravleva, I., Churazov, E., Arévalo, P., et al. 2016, MNRAS, 485, 2902
Zhuravleva, I., Churazov, E., Schekochihin, A. A., et al. 2014, Natur, 515, 85
Zhuravleva, I. V., Churazov, E. M., Sazonov, S. Y., Sunyaev, R. A., &
   Dolag, K. 2011, AstL, 37, 141
ZuHone, J., Miller, E. D., Bulbul, E., & Zhuravleva, I. 2017, arXiv:1708.07206
Zweibel, E. 1980, SoPh, 66, 305
```